PHYSICS

Superadiabatic quantum friction suppression in finite-time thermodynamics

Shujin Deng,[1] Aurélia Chenu,[2] Pengpeng Diao,[1] Fang Li,[1] Shi Yu,[1] Ivan Coulamy,[3,4] Adolfo del Campo,[3] Haibin Wu[1,5]*

Optimal performance of thermal machines is reached by suppressing friction. Friction in quantum thermodynamics results from fast driving schemes that generate nonadiabatic excitations. The far-from-equilibrium dynamics of quantum devices can be tailored by shortcuts to adiabaticity to suppress quantum friction. We experimentally demonstrate friction-free superadiabatic strokes with a trapped unitary Fermi gas as a working substance and establish the equivalence between the superadiabatic work and its adiabatic value.

INTRODUCTION

The quest for the optimal performance of thermal machines and efficient use of energy resources has motivated the development of finite-time thermodynamics. At the macroscale, thermodynamic cycles are operated in finite time to enhance the output power, at the expense of inducing friction and reducing efficiency. Analyzing the trade-off between efficiency and power has guided efforts in design and optimization (*1*, *2*). The advent of unprecedented techniques to experimentally control and engineer quantum devices at the nanoscale has shifted the focus to the quantum domain. A quantum engine is an instance of a thermal machine in which heat (*3*, *4*) and other quantum resources (*5*, *6*) can be used to produce work. The experimental realization of a single-atom heat engine (*7*) and a quantum absorption refrigerator (*8*) has been demonstrated using trapped ions. In the quantum domain, the adiabatic theorem (*9*) dictates that excitations are formed during fast driving of the working substance, leading to the emergence of quantum friction.

Trading efficiency and power remains a predominant strategy in finite-time quantum thermodynamics, for example, of ground-state cooling (*10*–*13*). In parallel, new efforts have been devoted to completely suppress friction in finite-time quantum processes.

A systematic way of achieving this goal is provided by shortcuts to adiabaticity (STA): fast nonadiabatic processes that reproduce adiabatic dynamics, for example, in the preparation of a target state (*14*). The use of STA provides an alternative approach in finite-time thermodynamics and has motivated proposals for superadiabatic thermal machines, operating at maximum efficiency and arbitrarily high output power (*15*–*18*). STA engineering is facilitated by counterdiabatic driving (*19*, *20*), whereby an auxiliary control field speeds up the evolution of the system through an adiabatic reference trajectory in a prescheduled amount of time. Experimental demonstrations of counterdiabatic driving have focused on effectively single-particle systems at zero temperature (*21*–*24*). Tailoring excitation dynamics is expected to be a daunting task in complex systems. However, efficient quantum thermal machines offering scalability require the superadiabatic control of the finite-time thermodynamics in many-particle systems (*17*). We report the suppression of quantum friction in the finite-time thermodynamics of a strongly coupled quantum fluid. In our experiment, we implement friction-free superadiabatic strokes with a unitary Fermi gas in an anisotropic time-dependent trap as a working medium.

The unitary regime is reached when the scattering length governing the short-range interactions in a spin-1/2 ultracold Fermi gas at resonance greatly surpasses the interparticle spacing (*25*). This strongly interacting state of matter is described by a nonrelativistic conformal field theory (*26*), with an emergent dynamical symmetry of scale invariance. The controllability of the external trap potential and interatomic interactions in this system allows for the preparation of well-defined many-body states and the precise engineering of time-dependent Hamiltonians. This provides unprecedented opportunities for studying strongly interacting nonequilibrium phenomena (*27*).

RESULTS

Our experiment probes the nonadiabatic expansion dynamics in an anisotropically trapped unitary quantum gas, a balanced mixture of ^{6}Li fermions in the lowest two hyperfine states $|\uparrow\rangle \equiv |F = 1/2, M_F = -1/2\rangle$ and $|\downarrow\rangle \equiv |F = 1/2, M_F = 1/2\rangle$. The experimental setup is similar to that in the studies of Deng *et al.* (*28*, *29*), with a new configuration of the dipole trap consisting of an elliptic beam generated by a cylindrical lens along the z axis and a nearly ideal Gaussian beam along the x axis (see the Supplementary Materials). The resulting potential has a cylindrical symmetry around x axis. This trap facilitates the control of the anisotropy and geometric frequency. Fermionic atoms are loaded into a cross-dipole trap used for evaporative cooling. A Feshbach resonance is used to tune the interactomic interaction to the unitary limit, reached at $B = 832$G. The system is initially prepared in a stationary state of a normal fluid, with $\omega_x(0) = 2\pi \times 1200$ Hz and $\omega_y(0) = \omega_z(0) = 2\pi \times 300$ Hz. The initial energy of Fermi gas at unitarity is $E = 0.8(0.1)\ E_F$, corresponding to a temperature $T = 0.25(0.02)\ T_F$, where E_F and T_F are the Fermi energy and temperature of an ideal Fermi gas, respectively.

The emergent scale invariance symmetry at unitarity (*30*) facilitates the realization of superadiabatic strokes by the counterdiabatic driving scheme (*31*, *32*). The work performed in a stroke induced by a modulation of the trap frequency can be described by a probability distribution (*33*). The mean work equals the difference between the energy of the atomic cloud brought out of equilibrium at the end of the stroke and its initial equilibrium value. Therefore, work performed by the cloud is negative, whereas work performed on it is positive. For a unitary dynamics, the emergent scaling symmetry at strong coupling (*30*) dictates the evolution

[1]State Key Laboratory of Precision Spectroscopy, East China Normal University, Shanghai 200062, P. R. China. [2]Massachusetts Institute of Technology, 77 Massachusetts Avenue, Cambridge, MA 02139, USA. [3]Department of Physics, University of Massachusetts, Boston, MA 02125, USA. [4]Departamento de Física, Universidade Federal Fluminense, Niterói, Rio de Janeiro, Brazil. [5]Collaborative Innovation Center of Extreme Optics, Shanxi University, Taiyuan 030006, China.
*Corresponding author. Email: hbwu@phy.ecnu.edu.cn

of the nonadiabatic energy in terms of the atomic cloud density profile. The density profile can be characterized using the collective coordinate operators

$$\hat{R}_x^2 = \sum_{i=1}^{N} \hat{x}_i^2,\ \hat{R}_y^2 = \sum_{i=1}^{N} \hat{y}_i^2,\ \hat{R}_z^2 = \sum_{i=1}^{N} \hat{z}_i^2 \tag{1}$$

Their expectation values determine the shape of the atomic cloud via the scaling factors $b_j^2(t) = \langle R_j^2(t)\rangle/\langle R_j^2(0)\rangle$, where, in each axis, $j = x, y, z$. Their evolution in time is governed by the coupled equations (*34*)

$$\ddot{b}_j(t) + \omega_j^2(t) b_j = \frac{\omega_{j,0}^2}{b_j \Gamma^{2/3}},\ j = x, y, z \tag{2}$$

where $\Gamma = b_x(t) b_y(t) b_z(t)$ is the scaling volume. Under slow driving, the adiabatic scaling factor reads $b_{j,ad}(t) = \omega_{j,0}/(\omega_j(t)\Gamma_{ad}^{1/3})$ and $\Gamma_{ad}(t) = \prod_j b_{j,ad}(t)$.

In characterizing the finite-time thermodynamics of isolated quantum systems, the ratio of the nonadiabatic and adiabatic mean energies plays a crucial role and is known as the nonadiabatic factor $Q^*(t) = \langle \hat{H}(t)\rangle/\langle \hat{H}(t)\rangle_{ad}$ (*35*, *36*). For a unitary anisotropic Fermi gas, the nonadiabatic factor is given by (see the Supplementary Materials)

$$Q^*(t) = \Gamma_{ad}^{2/3}(t)\left[\frac{1}{2\Gamma^{2/3}} + \frac{1}{6}\sum_{j=x,y,z}\frac{\dot{b}_j^2 + \omega_j^2(t) b_j^2}{\omega_{j,0}^2}\right] \tag{3}$$

and determines the nonadiabatic mean work

$$\langle W(t)\rangle = (Q^*(t)/\Gamma_{ad}^{2/3}(t) - 1)\langle H(0)\rangle \tag{4}$$

Quantum friction is evidenced during dynamical processes with values of $Q^*(t) > 1$. To suppress friction, the counterdiabatic driving technique (*19*, *20*) can be exploited in combination with dynamical scaling laws (*31*, *32*) to set $Q^* = 1$. We refer to this superadiabatic control as local counterdiabatic driving (LCD). To implement it, we first identify a desirable reference trajectory of the trap frequencies $\omega_j(t)$. We next design an STA protocol with modified frequencies $\Omega_j(t)$ that reproduces in an arbitrary prescheduled time t_f the final state that would correspond to the adiabatic evolution for $\omega_j(t)$. To this end, we choose a reference modulation of the trap, specifically

$$\omega_j(t) = \omega_j(0)\{1 + (b_{f,j} - 1)[10\tau^3 - 15\tau^4 + 6\tau^5]\} \tag{5}$$

where $\tau = t/t_f$ and $b_{f,j} = \omega_j(t_f)/\omega_j(0)$ are set by the ratio of the initial and final target trap frequencies. The engineering of an STA by LCD requires the nonadiabatic modulation of the trap frequencies (see the Supplementary Materials)

$$\Omega_j^2(t) = \omega_j^2 - 2\left(\frac{\dot{\omega}_j}{\omega_j}\right)^2 + \frac{\ddot{\omega}_j}{\omega_j} + \frac{1}{4}\left(\frac{\dot{\nu}}{\nu}\right)^2 - \frac{1}{2}\frac{\ddot{\nu}}{\nu} + \frac{\dot{\omega}_j\dot{\nu}}{\omega_j\nu} \tag{6}$$

where $\nu(t) = [\omega_x(t)\omega_y(t)\omega_z(t)]^{1/3}$ denotes the geometric mean frequency. The frequencies $\Omega_j(t)$ thus satisfy the desired boundary conditions, $\Omega_j(0) = \omega_j(0)$, $\Omega_j(t_f) = \omega_j(t_f)$, and $\dot{\omega}_j(0) = \ddot{\omega}_j(t_f) = 0$, while ensuring $Q^*(t_f) = 1$. Although the LCD dynamics is nonadiabatic at intermediate stages, quantum friction is thus suppressed upon completion of the stroke of arbitrary duration t_f.

The time-dependent trap frequencies and trap anisotropy in experiments are precisely controlled according to Eq. 5 for the reference driving and using Eq. 6 for the LCD. To monitor the evolution along the process, after a chosen expansion time with the trap turned on, the trap is completely turned off and the cloud is probed by standard resonant absorption imaging techniques after a time-of-flight expansion time $t_{\mathrm{tof}} = 600$ μs. Each data point is obtained from averaging five runs of measurements with identical parameters. The time-of-flight density profile along the axial (radial) direction is fitted by a Gaussian function, from which we obtain the observed cloud size $\sigma_{z,\mathrm{obs}}(\sigma_{r,\mathrm{obs}})$. The in situ cloud size σ_z (σ_r) and scaling factors b_j during the STA are obtained from the observed value $\sigma_{z,\mathrm{obs}}$ ($\sigma_{r,\mathrm{obs}}$) scaled by a factor evaluated from the hydrodynamic expansion equation during a time t_{tof} (see the Supplementary Materials).

Nonadiabatic factor and the mean work in an expansion stroke

Figure 1 shows the expansion stroke of the unitary Fermi gas with $b_{f,x} = 1/4$ and $b_{f,y} = b_{f,z} = 1$ in $t_f = 800$ μs. The trap frequencies are changed from the initial values $\omega_x(0) = 2\pi \times 1200$ Hz and $\omega_y(0) = \omega_z(0) = 2\pi \times 300$ Hz to the target values $\omega_x(t_f) = 2\pi \times 300$ Hz and $\omega_y(t_f) = \omega_z(t_f) = 2\pi \times 300$ Hz in 800 μs. The Fermi gas is initially confined in an anisotropic harmonic trap with a frequency aspect ratio of 4. Because of the engineering of frequencies, the size of the cloud gas is mostly expanded in the x axis, with the changes in the y and z directions being small (Fig. 1B) during the driving processes. Although the Fermi gas is anisotropic during the nonadiabatic, LCD, it becomes isotropic at the final target state, in which both the frequency and cloud size aspect ratio are close to 1 [see Fig. 1, B (iii) and C (iii)]. The measured nonadiabatic factor $Q^*(t)$ and mean work during the expansion stroke are shown in Fig. 2. For the reference driving, the $Q^*(t)$ of the strongly interacting Fermi gas monotonically increases, witnessing quantum friction induced by excitations that emerge from the nonadiabatic dynamics. At time $t_f = 800$ μs, $Q^*(t_f)$ approaches to 1.17 for the experimental parameters (see brown dots in Fig. 2A). Quantum friction decreases the mean work of the stroke, $\kappa(t) = \langle W(t)\rangle/\hat{H}(0)$ (see Fig. 2B). By contrast, quantum friction is greatly suppressed with the LCD scheme. $Q^*(t)$ reduces to 1 after completion of the superadiabatic stroke (see blue dots in Fig. 2A), revealing that it is a friction-free process. Using STA by LCD thus allows reaching $Q^*(t_f) = 1$, enhancing the work output. Its maximum value is reached at t_f and is determined by the geometric mean frequency according to

$$\langle W(t_f)\rangle_{\mathrm{LCD}} = \left[\left(\frac{\nu(t_f)}{\nu(0)}\right)^{1/3} - 1\right]\langle \hat{H}(0)\rangle \tag{7}$$

The measured value of the mean work κ in the experiment is about −0.37 in units of $\langle \hat{H}(0)\rangle$ (see blue dots in Fig. 2B), which is in very good agreement with the theoretical prediction, $(2^{-2/3} - 1) = -0.370$. Compared to the case of reference driving process, the mean work in the LCD process is increased by nearly 42.3%.

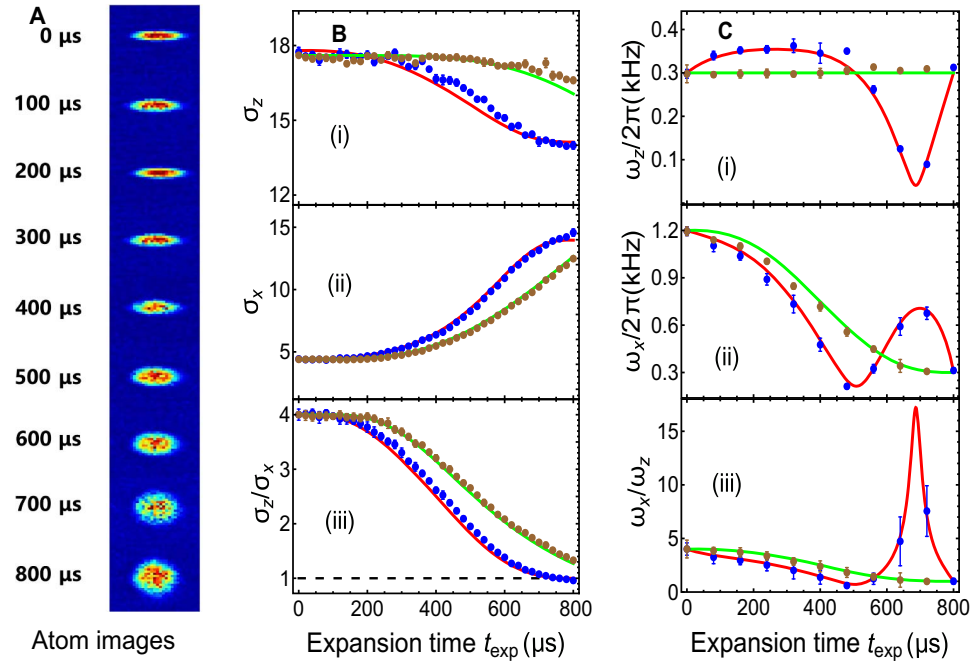

Fig. 1. Superadiabatic expansion stroke. The expansion stroke of the unitary Fermi gas for STA of LCD and reference driving case with $b_{f,x} = 1/4$, keeping $b_{f,y} = b_{f,z} = 1$ in $t_f = 800$ μs: the atom images of LCD (**A**), the measured cloud size and cloud aspect ratio (**B**), and the measured frequencies and frequency aspect ratio (**C**). Blue and brown dots are the measured results for LCD and reference driving case, respectively. The red and green lines are theoretical predictions. The black dashed line represents an aspect ratio of 1, indicating an isotropic trap for Fermi gas. Error bars represent the SD of the statistic.

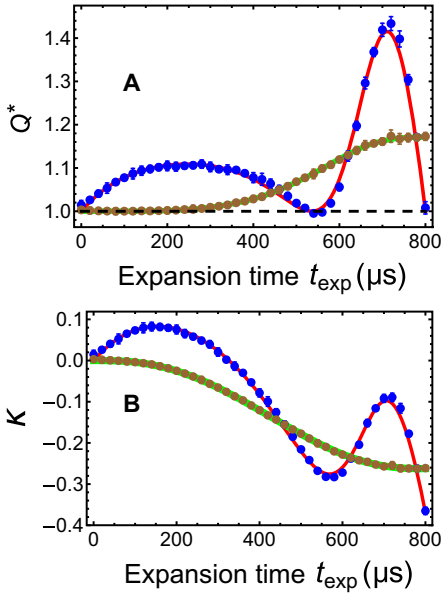

Fig. 2. Nonadiabatic factor Q^* and the mean work κ in an expansion stroke. Nonadiabatic factor Q^* (**A**) and the mean work (**B**) in an expansion stroke. Blue and brown dots denote the measured data for STA of LCD and nonadiabatic reference driving case, whereas the red and green lines are the corresponding theoretical predictions. $\kappa(t) = \langle W(t)\rangle / \langle \hat{H}(0)\rangle$ is the ratio of the mean work and the initial energy. The black dashed line represents $Q^* = 1$ where there is no quantum friction. Error bars represent the SD of the statistic.

Expansion stroke with the change of geometric mean frequency

As seen from Eq. 7, in an STA by LCD, quantum friction is suppressed, and the final mean work depends only on the ratio of geometric mean frequency between the initial state and the target state. For processes satisfying $\nu(t_f) = \nu(0)$, such as a change of the anisotropy of the cloud, the mean work vanishes. We verify this prediction experimentally. The strongly interacting Fermi gas is first prepared in a quantum state with frequencies of $\omega_x(0) = 2\pi \times 1200$ Hz and $\omega_y(0) = \omega_z(0) = 2\pi \times 300$ Hz. Then, following Eq. 5, the trap frequencies are changed to $\omega_x(t_f) = \omega_y(t_f) = \omega_z(t_f) = 2\pi \times (\prod_j \omega_j(0))^{1/3} = 2\pi \times 476.22$ Hz, modifying the aspect ratio of the cloud. The measured nonadiabatic factor $Q^*(t)$, mean work, and cloud expansion images are shown in Fig. 3. It is apparent that there is no friction $Q^*(t_f) = 1$ (see blue dots in Fig. 3A) and that the mean work vanishes $W(t_f) = 0$ (see blue dots in Fig. 3B) when manipulating the quantum state using STA by LCD. For the nonadiabatic reference driving, quantum friction is, however, induced and causes $Q^*(t_f) > 1$ (see brown dots in Fig. 3A), signaling energy dispersion in the final state. The mean work is then increased to a positive value of $1.22\ \langle \hat{H}(0)\rangle$ (see brown dots in Fig. 3B).

Time-averaged deviation of the mean work

A global measure of the nonadiabatic character of a superadiabatic stroke can be quantified by the time-averaged deviation of the mean work $\langle W(t)\rangle$ from the adiabatic value $\langle W_{ad}(t)\rangle$ as a function of the total time t_f

$$\delta W = \frac{1}{t_f}\int_0^{t_f} dt[\langle W(t)\rangle - \langle W_{ad}(t)\rangle] \quad (8)$$

In the experiment, we measure the mean work deviation in both an STA based on LCD and a nonadiabatic reference protocol for the expansion strokes. The initial and final geometric frequencies are fixed to 4.8 and 1.2, respectively. The trap frequencies are changed from the

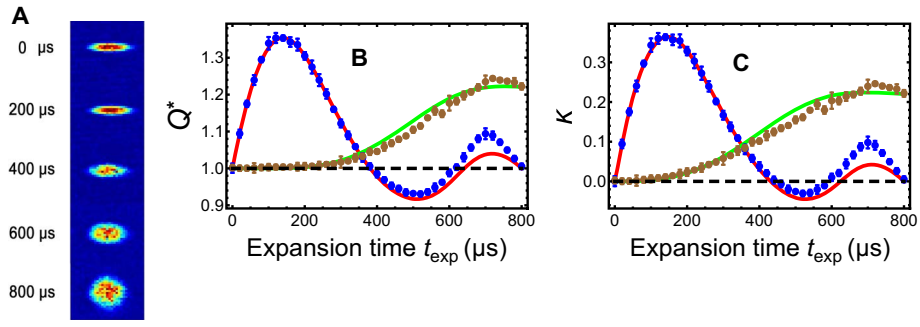

Fig. 3. Superadiabatic quantum friction suppression. Cloud expansion images (**A**), nonadiabatic factor Q^* (**B**), and mean work (**C**) of unitary Fermi gas during a change of the cloud aspect ratio that preserves the geometric mean frequency, $\nu(t_f) = \nu(0)$. Blue and brown dots represent the measured results for STA of LCD and nonadiabatic driving case, respectively. Red and green lines denote the corresponding theoretical predictions. Black dashed line denotes for the friction-free $Q^*(t_f) = 1$, and brown dashed line represents for the zero mean work $\kappa = 0$. Error bars represent the SD of the statistic.

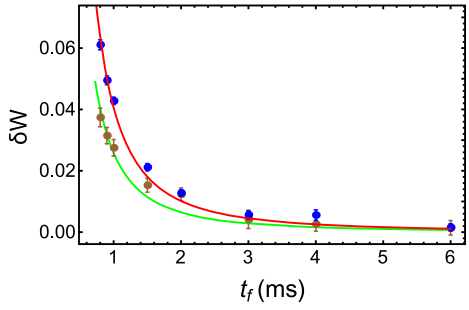

Fig. 4. Time-averaged mean work deviation δW in units of $\langle H(0)\rangle$ as a function of t_f. Blue and brown dots denote the measured data for STA by LCD and the nonadiabatic reference driving case, whereas the red and green lines are the fits with a function of $1/t_f^2$. Error bars represent the SD of the measurement data.

initial frequencies $\omega_x = 2\pi \times 1440$ Hz and $\omega_y = \omega_z = 2\pi \times 300$ Hz to $\omega_x = 2\pi \times 360$ Hz and $\omega_y = \omega_z = 2\pi \times 300$ Hz in different time t_f. For STA by LCD, the mean work $\langle W(t_f)\rangle$ matches the adiabatic value and does not change no matter how short the time t_f is. However, the evolution of $\langle W(t)\rangle$ along the protocol, for $t < t_f$, reflects the amplitude of the excess work needed to implement STA at different stages. The measured results for the time-averaged deviation δW are shown in Fig. 4. The shorter the time t_f, the greater the deviation of mean work δW. The solid curves are the fits with a power-law $1/t_f^2$ as a function of the duration of the stroke t_f.

DISCUSSION

The experiments presented here demonstrate the suppression of quantum friction and enhancement of the mean work output in superadiabatic strokes with a strongly interacting quantum fluid as a working medium. The control of the finite-time quantum thermodynamics is achieved using STA that exploits the emergent scale invariance of a unitary Fermi gas. In combination with cooling and heating steps, superadiabatic strokes can be used to engineer quantum heat engines and refrigerators (*15*–*18*, *37*, *38*), for example, based on a quantum Otto cycle, that operate at maximum efficiency with high output and cooling power.

MATERIALS AND METHODS

A laser system of 2.5-W laser output with Raman fiber amplifier and intracavity frequency doubler was used to realize a large–atom number magneto-optical trap (MOT) of ^{6}Li. After the MOT loading and cooling stage, an optical pumping process was performed, and a balanced mixture of atoms in the two lowest hyperfine states was prepared.

The cold atoms were loaded into an optical dipole trap formed by a single beam of a fiber laser operating at 1070 nm. A forced evaporation was first performed to cool atoms to quantum degeneracy in an external magnetic field at 832 G. Then, the atoms were transferred to a specially designed optical crossed dipole trap, which consists of two orthogonal far-off resonance laser beams (see the Supplementary Materials). The first beam, which is focused by a pair of cylindrical lens, propagated along the horizontal direction (z axis) and provided the more tight confinement in the x direction. The second beam with a nearly perfect Gaussian profile, perpendicular to the first beam, propagated along the vertical beam (x direction). The trap frequency aspect ratio was controlled by precisely adjusting the power ratio of the two beams.

Parametric resonance in the noninteracting Fermi gas was used to measure the trap frequencies. The roundness of the optical trap beams and the axes of the magnetic potential were carefully adjusted and aligned. The anharmonicity in the trapping potential was corrected from the trap depth and the energy. The anharmonicity in the experiment was smaller than 2%.

The system of Fermi gas was initially prepared in a stationary state with a dimensionless temperature $T/T_F \approx 0.25$, where T_F is the Fermi temperature. Subsequently, two independent acousto-optic modulators, which are controlled by two 16-bit arbitrary wave generators, precisely manipulated the trap frequents to follow either the STA of LCD or the reference driving scheme. An absorption image was taken with the time-of-flight to get the atomic cloud. The in situ cloud sizes were obtained from the measured value scaled by a factor evaluated from the hydrodynamic expansion equation (*28*, *29*, *39*, *40*).

SUPPLEMENTARY MATERIALS

Supplementary material for this article is available at http://advances.sciencemag.org/cgi/content/full/4/4/eaar5909/DC1

section S1. Finite-time thermodynamics of a unitary Fermi gas in a time-dependent anisotropic trap
section S2. Local counterdiabatic control of the finite-time thermodynamics of a unitary Fermi gas
section S3. Experiment methods
section S4. Expansion factor
section S5. Expansion and compression stroke
fig. S1. Experimental setup and procedure.
fig. S2. Determination of the cloud size $\langle\sigma_z\rangle$ obtained from the Gaussian fit of the density profile of the unitary Fermi gas for a time-of-flight $t_{tof} = 600$ μs.
fig. S3. Evolution of the nonadiabatic factor $Q^*(t)$ for the expansion and compression strokes.
fig. S4. Mean work $\kappa = \langle W(t)\rangle/\langle H(0)\rangle$ for both the expansion stroke and compression stroke.

fig. S5. Time evolution of the dimensionless factor $\bar{\kappa}$ for both the expansion and compression strokes, $\bar{\kappa} = (\langle W_{\rm exp}(t)\rangle - \langle W_{\rm comp}(t_f - t)\rangle)/\langle H(0)\rangle_1 - 1$.

REFERENCES AND NOTES

1. F. L. Curzon, B. Ahlborn, Efficiency of a Carnot engine at maximum power output. *Am. J. Phys.* **43**, 22–24 (1975).
2. B. Andresen, P. Salamon, R. S. Berry, Thermodynamics in finite time. *Phys. Today* **37**, 62–70 (1984).
3. R. Alicki, The quantum open system as a model of the heat engine. *J. Phys. A Math. Gen.* **12**, L103 (1979).
4. R. Kosloff, A quantum mechanical open system as a model of a heat engine. *J. Chem. Phys.* **80**, 1625–1631 (1984).
5. M. O. Scully, M. S. Zubairy, G. S. Agarwal, H. Walther, Extracting work from a single heat bath via vanishing quantum coherence. *Science* **299**, 862–864 (2003).
6. J. Roßnagel, O. Abah, F. Schmidt-Kaler, K. Singer, E. Lutz, Nanoscale heat engine beyond the Carnot limit. *Phys. Rev. Lett.* **112**, 030602 (2014).
7. J. Roßnagel, S. T. Dawkins, K. N. Tolazzi, O. Abah, E. Lutz, F. Schmidt-Kaler, K. Singer, A single-atom heat engine. *Science* **352**, 325–329 (2016).
8. G. Maslennikov, S. Ding, R. Hablutzel, J. Gan, A. Roulet, S. Nimmrichter, J. Dai, V. Scarani, D. Matsukevich, Quantum absorption refrigerator with trapped ions. arXiv:1702.08672 (2017).
9. T. Kato, On the adiabatic theorem of quantum mechanics. *J. Phys. Soc. Jpn.* **5**, 435–439 (1950).
10. E. Geva, R. Kosloff, On the classical limit of quantum thermodynamics in finite time. *J. Chem. Phys.* **97**, 4398–4412 (1992).
11. Y. Rezek, R. Kosloff, Irreversible performance of a quantum harmonic heat engine. *New J. Phys.* **8**, 83 (2006).
12. N. Shiraishi, K. Saito, H. Tasaki, Universal trade-off relation between power and efficiency for heat engines. *Phys. Rev. Lett.* **117**, 190601 (2016).
13. R. Onofrio, Physics of our days: Cooling and thermometry of atomic Fermi gases. *Phys. Usp.* **59**, 1129 (2016).
14. E. Torrontegui, S. Ibáñez, S. Martínez-Garaot, M. Modugno, A. del Campo, D. Guéry-Odelin, A. Ruschhaupt, X. Chen, J. G. Muga, Shortcuts to adiabaticity. *Adv. At. Mol. Opt. Phys.* **62**, 117–169 (2013).
15. J. Deng, Q.-h. Wang, Z. Liu, P. Hänggi, J. Gong, Boosting work characteristics and overall heat engine performance via shortcuts to adiabaticity: Quantum and classical systems. *Phys. Rev. E* **88**, 062122 (2013).
16. A. del Campo, J. Goold, M. Paternostro, More bang for your buck: Super-adiabatic quantum engines. *Sci. Rep.* **4**, 6208 (2014).
17. M. Beau, J. Jaramillo, A. del Campo, Scaling-up quantum heat engines efficiently via shortcuts to adiabaticity. *Entropy* **18**, 168 (2016).
18. O. Abah, E. Lutz, Energy efficient quantum machines. *Europhys. Lett.* **118**, 40005 (2017).
19. M. Demirplak, S. A. Rice, Adiabatic population transfer with control fields. *J. Phys. Chem. A* **107**, 9937–9945 (2003).
20. M. V. Berry, Transitionless quantum driving. *J. Phys. A Math. Theor.* **42**, 365303 (2009).
21. M. G. Bason, M. Viteau, N. Malossi, P. Huillery, E. Arimondo, D. Ciampini, R. Fazio, V. Giovannetti, R. Mannella, O. Morsch, High-fidelity quantum driving. *Nat. Phys.* **8**, 147–152 (2012).
22. J. Zhang, J. H. Shim, I. Niemeyer, T. Taniguchi, T. Teraji, H. Abe, S. Onoda, T. Yamamoto, T. Ohshima, J. Isoya, D. Suter, Experimental implementation of assisted quantum adiabatic passage in a single spin. *Phys. Rev. Lett.* **110**, 240501 (2013).
23. Y.-X. Du, Z.-T. Liang, Y.-C. Li, X.-X. Yue, Q.-X. Lv, W. Huang, X. Chen, H. Yan, S.-L. Zhu, Experimental realization of stimulated Raman shortcut-to-adiabatic passage with cold atoms. *Nat. Commun.* **7**, 12479 (2016).
24. S. An, D. Lv, A. del Campo, K. Kim, Shortcuts to adiabaticity by counterdiabatic driving for trapped-ion displacement in phase space. *Nat. Commun.* **7**, 12999 (2016).
25. C. Chin, R. Grimm, P. Julienne, E. Tiesinga, Feshbach resonances in ultracold gases. *Rev. Mod. Phys.* **82**, 1225–1286 (2010).
26. Y. Nishida, D. T. Son, Nonrelativistic conformal field theories. *Phys. Rev. D* **76**, 086004 (2007).
27. W. Zwerger, *The BCS-BEC Crossover and the Unitary Fermi Gas* (Springer Berlin Heidelberg, 2012).
28. S.-J. Deng, P.-P. Diao, Q.-L. Yu, H.-B. Wu, All-optical production of quantum degeneracy and molecular Bose-Einstein condensation of ^{6}Li. *Chin. Phys. Lett.* **32**, 053401 (2015).
29. S. Deng, Z.-Y. Shi, P. Diao, Q. Yu, H. Zhai, R. Qi, H. Wu, Observation of the Efimovian expansion in scale-invariant Fermi gases. *Science* **353**, 371–374 (2016).
30. K. M. O'Hara, S. L. Hemmer, M. E. Gehm, S. R. Granade, J. E. Thomas, Observation of a strongly interacting degenerate Fermi gas of atoms. *Science* **298**, 2179–2182 (2002).
31. A. del Campo, Shortcuts to adiabaticity by counterdiabatic driving. *Phys. Rev. Lett.* **111**, 100502 (2013).
32. S. Deffner, C. Jarzynski, A. del Campo, Classical and quantum shortcuts to adiabaticity for scale-invariant driving. *Phys. Rev. X* **4**, 021013 (2014).
33. P. Talkner, E. Lutz, P. Hänggi, Fluctuation theorems: Work is not an observable. *Phys. Rev. E* **75**, 050102(R) (2007).
34. C. Menotti, P. Pedri, S. Stringari, Expansion of an interacting Fermi gas. *Phys. Rev. Lett.* **89**, 250402 (2002).
35. K. Husimi, Miscellanea in elementary quantum mechanics, II. *Prog. Theor. Phys.* **9**, 381–402 (1953).
36. J. Jaramillo, M. Beau, A. del Campo, Quantum supremacy of many-particle thermal machines. *New J. Phys.* **18**, 075019 (2016).
37. P. Salamon, K. H. Hoffmann, Y. Rezek, R. Kosloff, Maximum work in minimum time from a conservative quantum system. *Phys. Chem. Chem. Phys.* **11**, 1027–1032 (2009).
38. R. Kosloff, Y. Rezek, The quantum harmonic Otto cycle. *Entropy* **19**, 136 (2017).
39. C. Cao, E. Elliott, J. Joseph, H. Wu, J. Petricka, T. Schäfer, J. E. Thomas, Universal quantum viscosity in a unitary Fermi gas. *Science* **331**, 58–61 (2011).
40. E. Elliott, J. A. Joseph, J. E. Thomas, Anomalous minimum in the shear viscosity of a Fermi gas. *Phys. Rev. Lett.* **113**, 020406 (2014).

Acknowledgments

Funding: This research was supported by the National Key Research and Development Program of China (grant no. 2017YFA0304201), National Natural Science Foundation of China (grant nos. 11734008, 11374101, 91536112, and 11621404), Program of Shanghai Subject Chief Scientist (17XD1401500), the Shanghai Committee of Science and Technology (17JC1400500), University of Massachusetts Boston (project P20150000029279), and the John Templeton Foundation. **Author contributions:** S.D., P.D., F.L., S.Y., and H.W. carried out the experiment and analyzed the data. A.C., A.d.C., I.C., and S.D. developed the theory. S.D., A.d.C., and H.W. wrote the manuscript with input from all authors. **Competing interests:** The authors declare that they have no competing interests. **Data and materials availability:** All data needed to evaluate the conclusions in the paper are present in the paper and/or the Supplementary Materials. Additional data related to this paper may be requested from H.W. (hbwu@phy.ecnu.edu.cn).

Submitted 27 November 2017
Accepted 9 March 2018
Published 27 April 2018
10.1126/sciadv.aar5909

Citation: S. Deng, A. Chenu, P. Diao, F. Li, S. Yu, I. Coulamy, A. del Campo, H. Wu, Superadiabatic quantum friction suppression in finite-time thermodynamics. *Sci. Adv.* **4**, eaar5909 (2018).

ScienceAdvances

Superadiabatic quantum friction suppression in finite-time thermodynamics

Shujin DengAurélia ChenuPengpeng DiaoFang LiShi YuIvan CoulamyAdolfo del CampoHaibin Wu

Sci. Adv., 4 (4), eaar5909. • DOI: 10.1126/sciadv.aar5909

Science Advances (ISSN 2375-2548) is published by the American Association for the Advancement of Science. 1200 New York Avenue NW, Washington, DC 20005. The title *Science Advances* is a registered trademark of AAAS.